

SUPPLEMENTARY INFORMATION

A Simple Two-Dimensional Model System to Study Electrostatic-Self-Assembly

Rebecca Cademartiri, Claudiu A. Stan, Vivian M. Tran, Evan Wu, Liam Frair, Daryl Vulis,

Logan W. Clark, Simon Tricard, and George M. Whitesides*

Department of Chemistry and Chemical Biology, Harvard University,

Cambridge, MA 01238 USA


Abstract. This supplementary information file contains: i) a selection of materials (including the ones we used in our experiments) ranked in a triboelectric series; ii) a description of the experimental apparatus; iii) a detailed description of the image analysis procedures; and iv) additional data and images describing the effect of dyeing the objects, the stability of charge, the assembly process under different types of agitation, mechanisms of structural rearrangements, the self-assembly of Teflon and Nylon spheres mixed in different proportions, and the effect of using gold instead of aluminum dishes.

* corresponding author, e-mail: gwhitesides@gmwgroup.harvard.edu

1. Triboelectric series for the materials investigated in our study

Table ST1 shows a triboelectric series, adapted from Diaz *et al.*,¹ that lists several common materials and includes all materials we used in self-assembly experiments. If available, the trademark name of these materials or their common technical abbreviation is listed between brackets. The materials used in this paper are printed in red.

Table ST1 The triboelectric series.



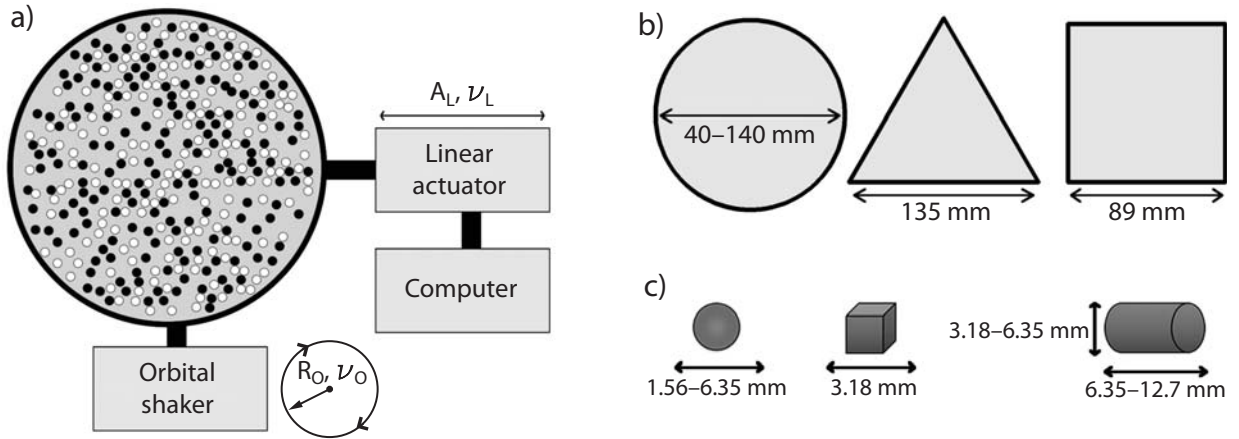
More positive	Glass
	Polyoxymethylene (Delrin)
	Polyamide (Nylon)
	Silica
	Aluminum
	Polyvinyl alcohol
	Paper
	Cotton
	Steel
	Wood
	Poly(methyl methacrylate) (PMMA)
	High-density polyethylene (HDPE)
	Gold
	Polyethylene terephthalate (PET, Mylar)
	Natural rubber
	Polystyrene (PS)
	Polypropylene (PP)
	Polyamide-imide (Torlon)
	Polyvinyl chloride (PVC)
More negative	Polytetrafluorethylene (PTFE, Teflon)

2. Experimental apparatus

Fig. S1(a) shows a schematic drawing of the experimental apparatus. We used the orbital shaker or the linear actuator separately, or combined them to generate a pseudo-random motion.² The amplitude (A_L) and linear frequency (ν_L) of the linear actuator was controlled via a computer interface; the orbital shaker had a fixed radius of gyration (R_O) characteristic for the type of shaker used, and variable frequency (ν_O). The drawing of the dish indicates the typical spatial arrangement of a mixture of two types of spheres before mixing. A glove bag (not shown) surrounded the actuator and the dish to maintain low humidity.

The dishes had circular, square and equilateral-triangular shapes (Fig. S1(b)). We used only one size of triangular and square dishes, designed to have the same surface area as a circular dish with a diameter of 100 mm, and circular dishes with different diameters. The objects that we used for self-assembly experiments (Fig. S1(c)) were made from polymeric materials, were millimeter-sized, and had spherical, cubic and cylindrical shapes.

Fig. S1 The experimental apparatus.



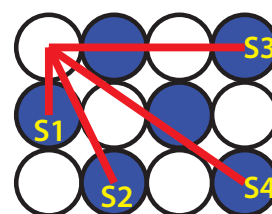
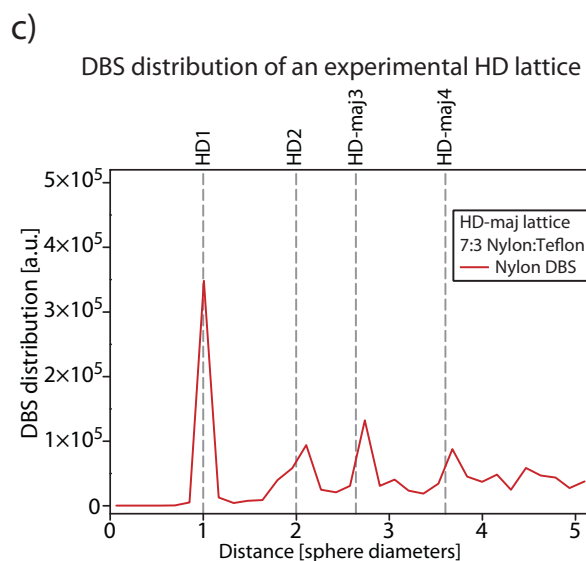
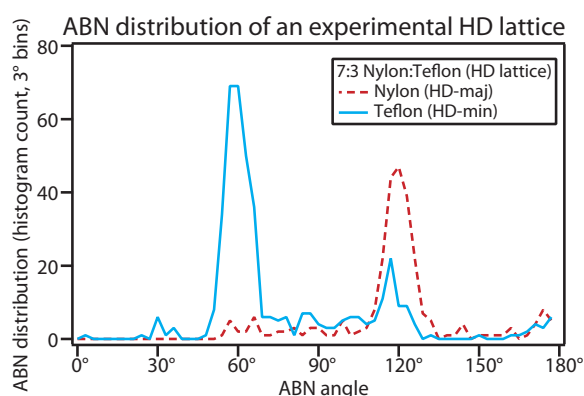
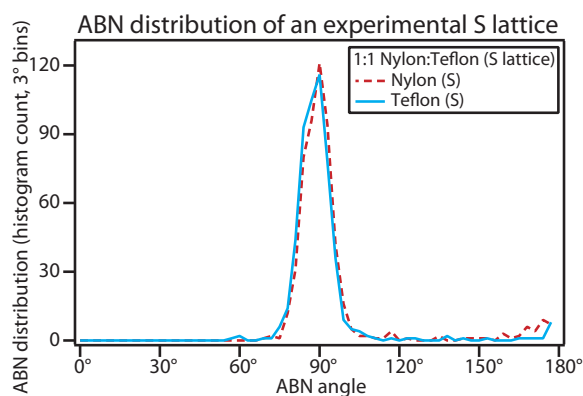
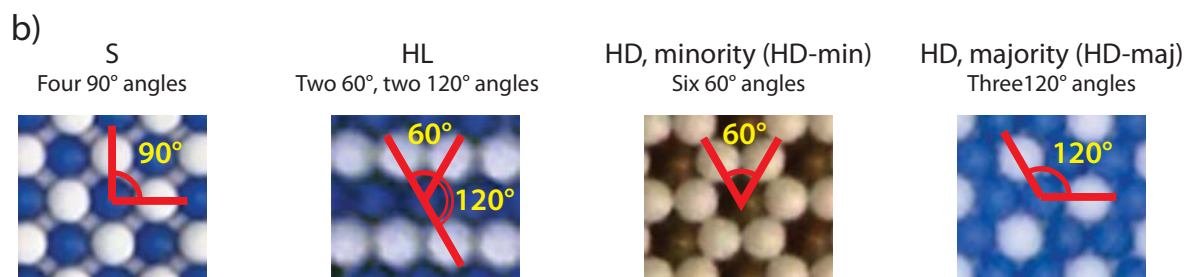
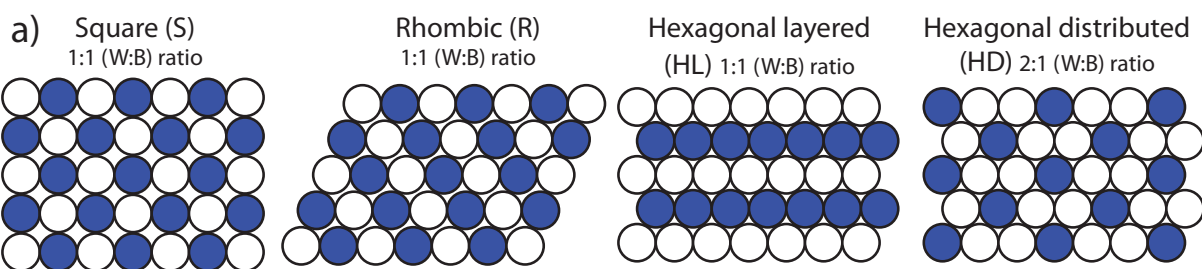
3. The quantitative analysis of lattice structure types.

The sphere assemblies formed in our experiments were rarely organized as a monolithic 2D crystal with a single type of lattice symmetry. We therefore developed a basic procedure to quantify the type and degree of crystalline order. This procedure uses images of the system as raw data to produce two types of distributions: one of the angles between neighbors (ABN) and one of the distances between spheres of different types (DBS). Analysis of the ABN and DBS distributions produces analytical measures of the degree and type of crystalline order, such as the proportion of spheres incorporated in a square crystalline lattice.

The image analysis and the calculation of ABN and DBS distributions were described in the main paper. The procedures for quantifying the types and degrees of crystalline order were based on the observation that mixtures of two types of spheres could form four types of crystalline structures, as shown in Fig. S2(a): square (S), rhombic (R), hexagonal-layered (HL), and hexagonal-distributed (HD). The S, R and HL types have a 1:1 stoichiometry, and the HD type has a 2:1 stoichiometry. For the purpose of analysis, we had to distinguish in the case of HD lattices whether the analyses were done in respect with the less abundant (minority) type of sphere (HD-min) or with the more abundant (majority) type of sphere (HD-maj) (Fig. S2(b)). Square and layered-hexagonal lattices can be regarded as special cases of the rhombic lattice, in which the angle formed by one sphere and two of its closest neighbors of the other type is 90° and 60° , respectively. In our classification, a rhombic lattice is characterized by angles between 60° and 90° .

The interpretation of the ABN distribution (Fig. S2(b)) is based on the fact that in S, HL, and HD lattices the angles between neighbors have precise and distinct values. Rhombic lattices cannot be distinguished using our basic method because the rhombic angle between neighbors does not have a precise value. We used the numbers of angles near 60° , 90° , and 120° (n_{60} , n_{90} , n_{120}) to determine the number of spheres which were part of S, HL, HD-maj, and HD-min lattices (n_S , n_{HL} , n_{HD-maj} , n_{HD-min}), according to equations SE 1–4. The fraction of spheres in a given type of lattice was obtained by dividing these numbers by the total number of spheres. Our analysis does not treat separately spheres at the boundary of a crystal, and thus underestimates the fraction of spheres in a given type of lattice.

Fig. S2 Mathematical analysis of the crystalline order of assemblies.



Lattice	Peak location [sphere diameters]			
	1	2	3	4
S	1.00	2.24	3.00	3.61
HD-min	1.00	2.00	2.65	3.61
HD-maj	1.00	2.00	2.65	3.61
HL	1.00	1.73	2.65	3.00
R	1.00	1.74-2.23	N/A	N/A

$$n_s = \frac{n_{90}}{4} \quad \text{SE(1)}$$

$$n_{HL} = \frac{(n_{60} + n_{120}) - |(n_{60} - n_{120})|}{4} \quad \text{SE(2)}$$

$$n_{HD-min} = \max\left(0, \frac{(n_{60} - n_{120})}{6}\right) \quad \text{SE(3)}$$

$$n_{HD-maj} = \max\left(0, \frac{(n_{120} - n_{60})}{3}\right) \quad \text{SE(4)}$$

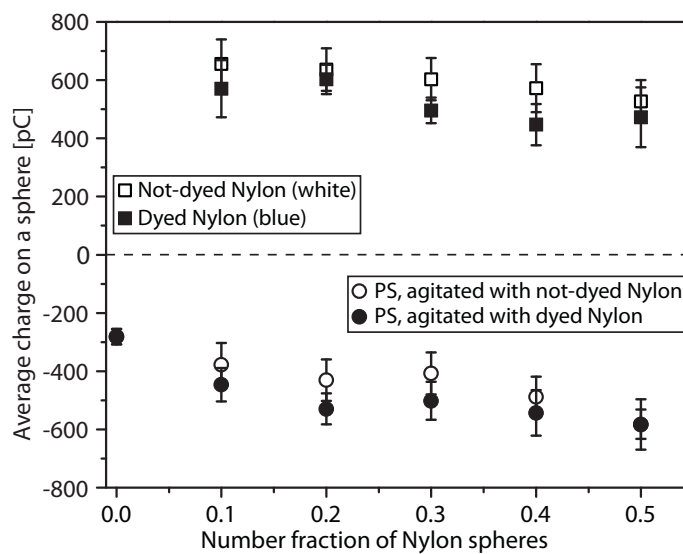
For the actual calculation of n_{60} , n_{90} , n_{120} we used finite-sized bins of angles with a half-width of 6° , centered on the exact angle values. We chose a half-width of 6° because it represents half the difference between the angles characteristic of pentagonal (72°) and hexagonal (60°) symmetries.

To interpret the DBS distribution (Fig. S2(c)), we calculated the locations of the nearest, second-nearest, third-nearest, and fourth-nearest neighbors of the different type of material, for all types of lattices; these values are listed in the table that is part of Fig. S2, and the location of these neighbors in a square lattice is indicated in the schematic above the table. Our basic DBS analysis cannot identify rhombic lattices because the location of neighbors and the ranking of their distances depends on the characteristic angle of the rhombic lattice. Square, layered-hexagonal, and distributed-hexagonal lattices can be distinguished by the second peak in the DBS, which corresponds to second-nearest neighbors. We note that in the experimentally determined DBS distributions, the peaks were usually not located at the exact distances listed in the table; in most cases this discrepancy is an artifact of the finite bin size that we used in the calculation of the histograms of the DBS distribution.

4. Supplementary data.

The effect of dyeing the objects on their triboelectric properties. We checked the effect of dyeing Nylon spheres blue by comparing the steady-state charges acquired by dyed and not-dyed spheres (Fig. S3), when agitated with PS spheres in different proportions (40 spheres in total) on a 40-mm gold-coated dish. We measured the charges after three minutes of agitation. The effect of dyeing was not statistically significant.

Fig. S3 Charging of dyed and not-dyed Nylon spheres.



The stability of charge after the end of agitation. We evaluated the stability of charge using a system of self-assembled Nylon and Teflon spheres (170 spheres of each type, agitated for three minutes in a 100-mm aluminum dish). After the end of agitation we kept the system in the glove bag (4% relative humidity) and we measured the charge of Nylon and Teflon spheres immediately, and at 1, 4, 22, and 47 hours after the end of agitation. For each charge measurement we averaged data from 10 spheres of each type. The charge of Nylon spheres decreased by $25 \pm 15\%$ after the first four hours and then remained constant; the charge of Teflon spheres did not change.

Fig. S4 The stability of charge.

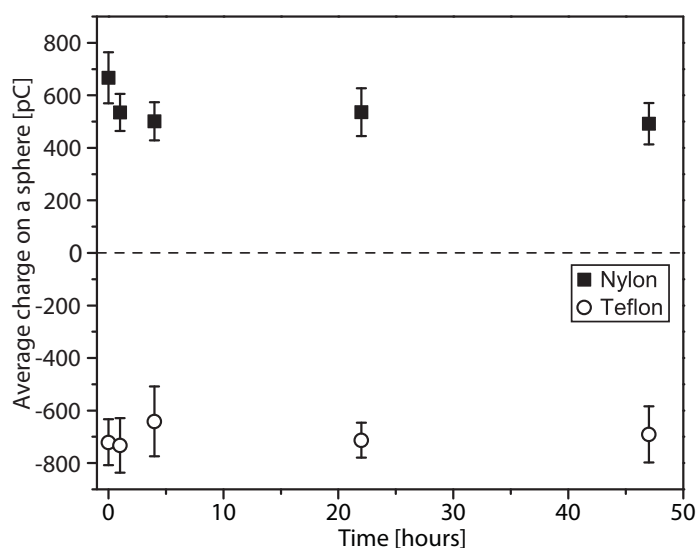
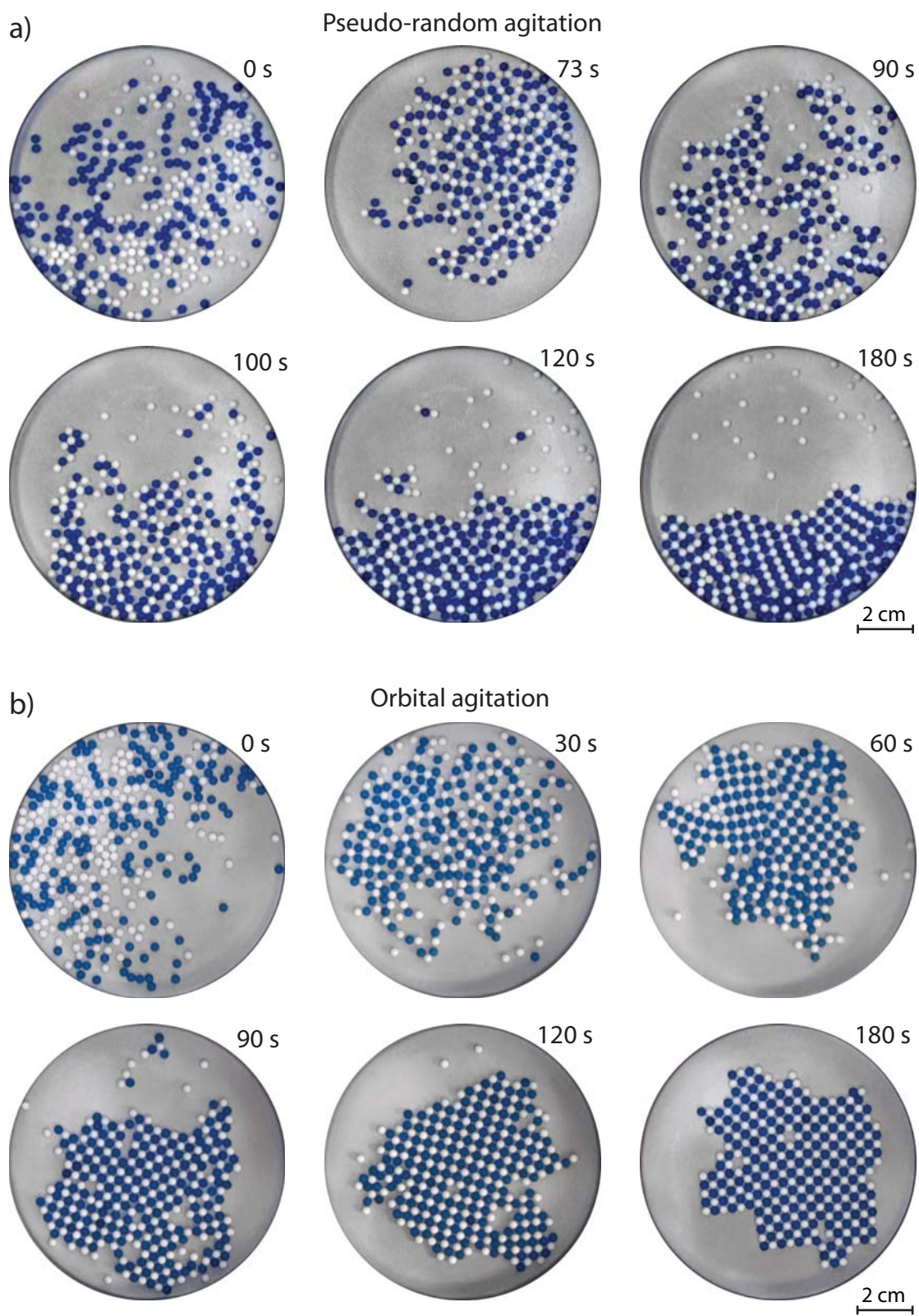
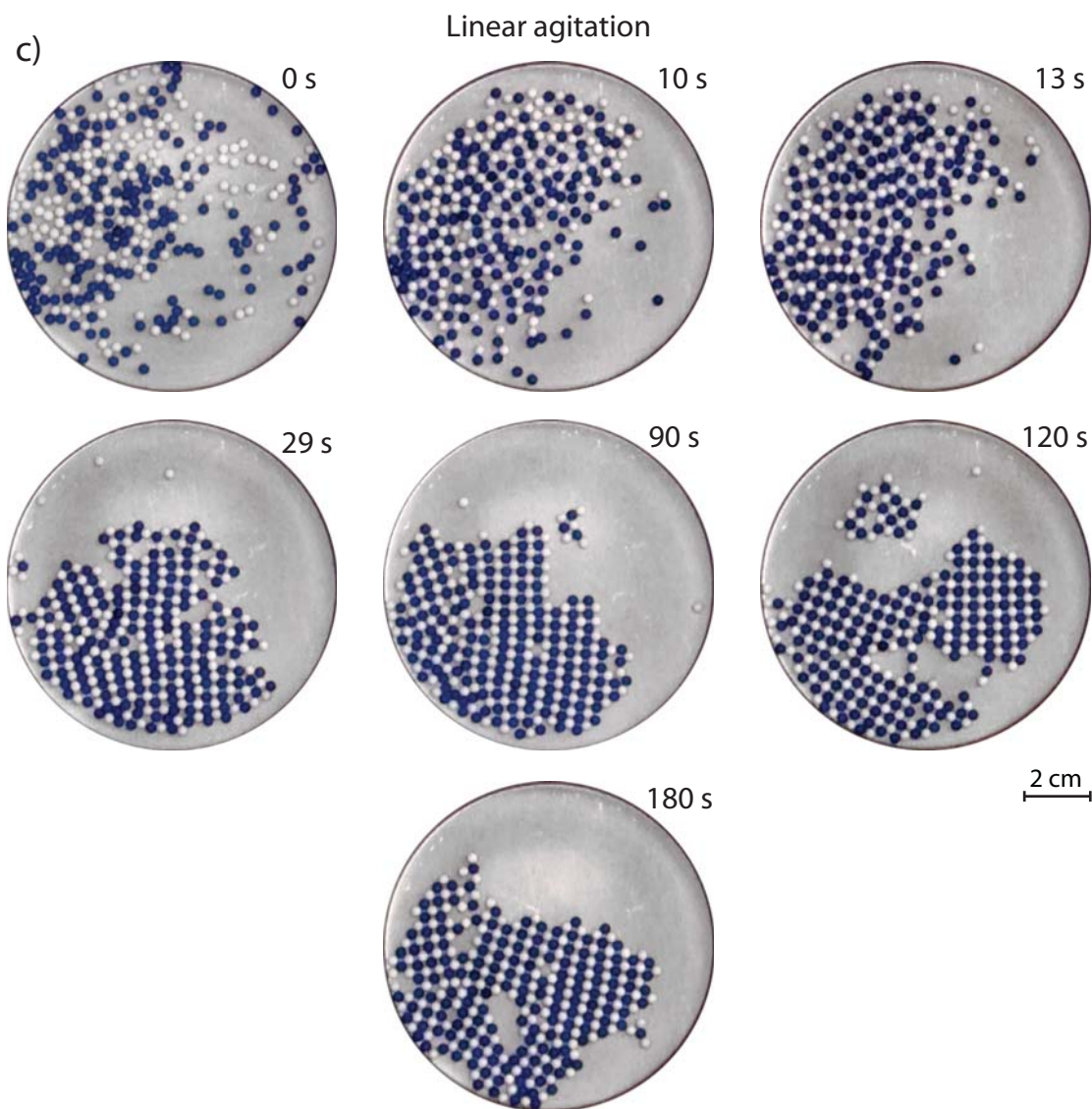


Fig. S5 Evolution of self-assembly during different types of agitation.

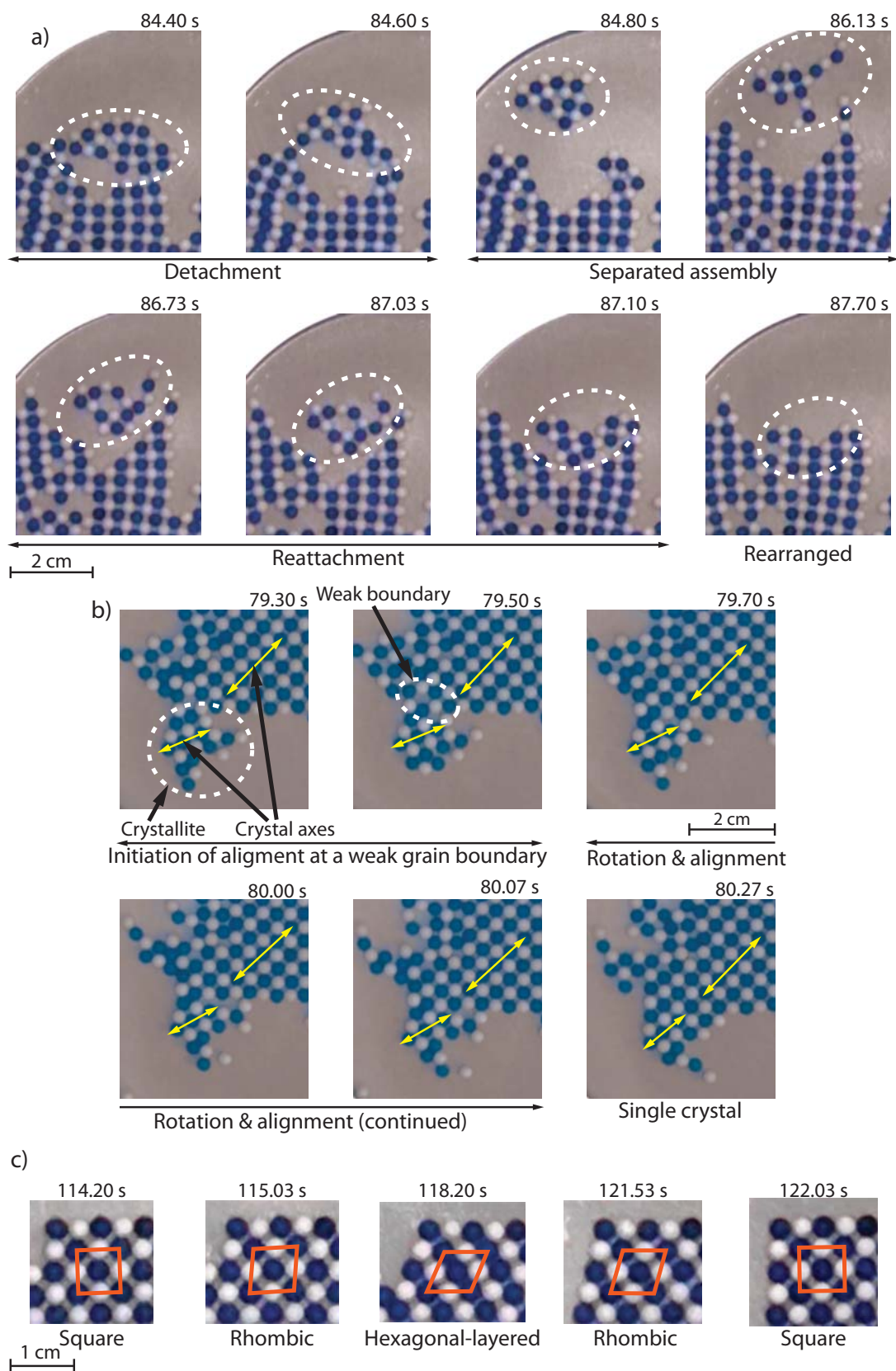




For all experiments in which we investigated the type of agitation (Fig. S5), we used a mixture of 170 Nylon and 170 Teflon spheres in an aluminum dish with a diameter of 100 mm.

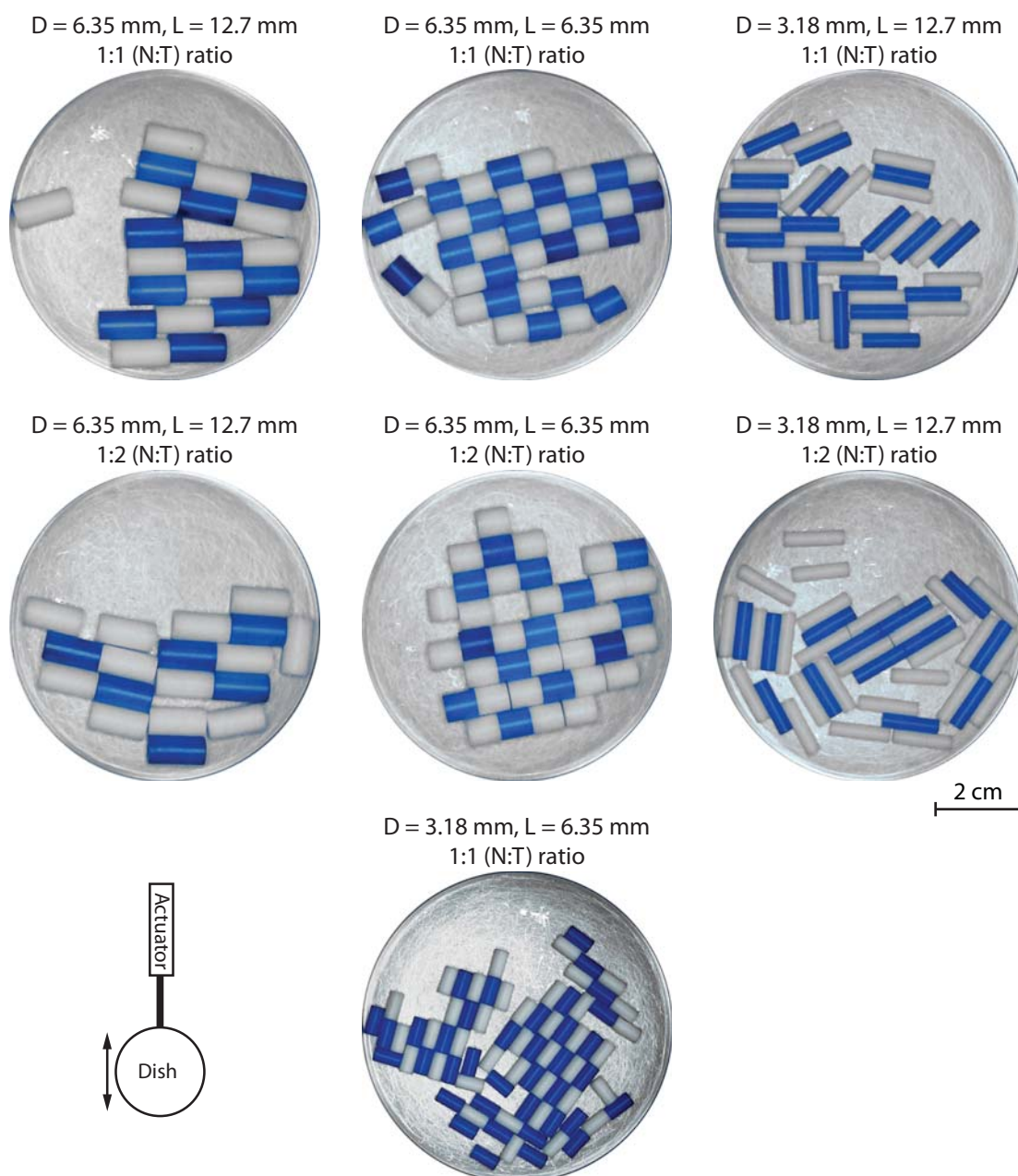
Rearrangement mechanisms. Images of three types of assembly rearrangement are shown in Fig. S6: detachment and reattachment of crystallites (Fig. S6(a)), sliding and twisting along crystallite boundaries (Fig. S6(b)), and changes in the symmetry of the lattice (Fig. S6(c)). The type of agitation was linear for the first and third types of rearrangement and orbital for the second; the other experimental conditions were the same as those used in the investigation of the type of agitation.

Fig. S6 Assembly rearrangement mechanisms.



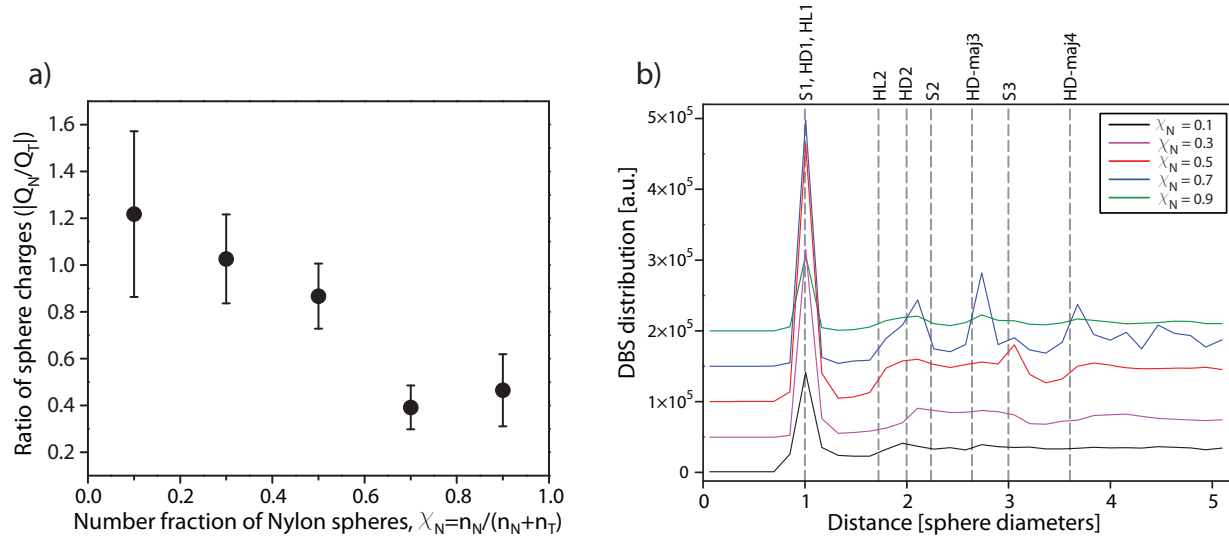
The self-assembly of cylinders. Images of assemblies formed by identically-shaped cylinders of Nylon and Teflon are shown in Fig. S7. We used an aluminum dish with a diameter of 70 mm shaken with a linear motion, and we tested both 1:1 (Nylon:Teflon) and 1:2 ratios of the number of objects. Compared with spheres and cubes, the cylinders were less likely to form crystalline structures; their tendency to crystallize decreased as their aspect ratio (length/diameter) increased.

Fig. S7 Self-assembly of tribocharged cylinders.



The self-assembly of Nylon and Teflon spheres mixed in different proportions. Fig. S8 shows additional data for experiments in which we varied the ratio of numbers of Nylon and Teflon spheres (Fig. 11 in the main paper). The electrical charge of Nylon spheres decreased as their proportion increased (Fig. S8(a)). The DBS distributions for the five cases (Fig. S8(a)) illustrate the differences between these cases. The most ordered structures, according to the DBS analysis, were those formed at Nylon fraction numbers, χ_N , of 0.5 and 0.7. Although visual inspection of images of the assemblies suggest that the assembly for which $\chi_N = 0.5$ is the most ordered, the DBS distribution for $\chi_N = 0.7$ has the sharpest peaks. The absence of sharper peaks in the former case can be explained by the fact that the assembly formed is a mixture of S, R, and HL structures. Precisely localized peaks characteristic of S and HL structures overlapped with the broader features characteristic of R structures (which exhibited a range of symmetry angles) and thus produced a relatively flat DBS distribution.

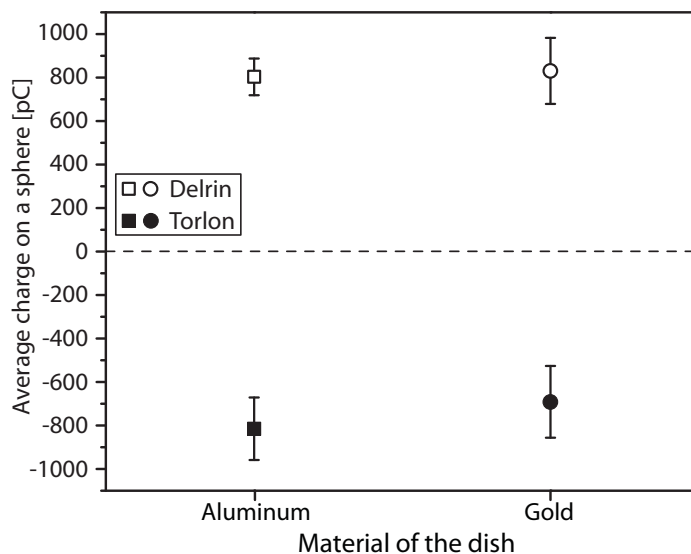
Fig. S8 Charge and crystalline order of Nylon:Teflon assemblies with different ratios of number of spheres.



Comparison of self-assembly in gold-coated and aluminum dishes. In our previous studies³⁻⁵ we used gold-coated dishes; here we performed most of our experiments in dishes machined from solid aluminum. Unlike gold, aluminum is coated with a layer of aluminum oxide under normal atmospheric conditions; it is difficult therefore to define precisely the properties of the “aluminum surface” under atmospheric conditions. We chose nevertheless to use aluminum instead of gold-coated dishes, because gold-coated dishes were prone to degradation by flaking and wear of the thin gold coating.

Our comparisons of self-assembly in aluminum and gold-coated dishes showed that the assemblies were similar, and the charges acquired by a given type of object on gold and aluminum were within the standard deviation of charge measurements. Fig. S9 shows the average steady-state charges of Delrin and Torlon spheres (20 spheres each in 40-mm dishes), measured after three minutes of agitation.

Fig. S9 Charge acquired by Delrin and Torlon spheres on gold and aluminum surfaces.



5. References

1. A. F. Diaz and R. M. Felix-Navarro, *J. Electrostat.*, 2004, **62**, 277-290.
2. M. Reches, P. W. Snyder and G. M. Whitesides, *P. Natl. Acad. Sci. USA*, 2009, **106**, 17644-17649.
3. B. A. Grzybowski, A. Winkleman, J. A. Wiles, Y. Brumer and G. M. Whitesides, *Nat. Mater.*, 2003, **2**, 241-245.
4. G. K. Kaufman, M. Reches, S. W. Thomas, J. Feng, B. F. Shaw and G. M. Whitesides, *Appl. Phys. Lett.*, 2009, **94**, 044102.
5. G. K. Kaufman, S. W. Thomas, M. Reches, B. F. Shaw, J. Feng and G. M. Whitesides, *Soft Matter*, 2009, **5**, 1188-1191.